Articles

Roles of Noncoordinated Aromatic Residues in Redox Regulation of Cytochrome c_3 from *Desulfovibrio vulgaris* Miyazaki F†

Yuki Takayama,‡ Erisa Harada,‡,§ Rie Kobayashi,|| Kiyoshi Ozawa,||,⊥ and Hideo Akutsu*,‡

Institute for Protein Research, Osaka University, Yamadaoka, Suita 565-0871, Japan, Japan Biological Informatics Consortium, Chuo-ku, Tokyo 104-0032, Japan, and Faculty of Engineering, Yokohama National University, Hodogaya-ku, Yokohama 240-8501, Japan

Received March 6, 2004; Revised Manuscript Received June 18, 2004

ABSTRACT: The roles of aromatic residues in redox regulation of cytochrome c_3 were investigated by site-directed mutagenesis at every aromatic residue except for axial ligands (Phe20, Tyr43, Tyr65, Tyr66, His67, and Phe76). The mutations at Phe20 induced large chemical shift changes in the NMR signals for hemes 1 and 3, and large changes in the microscopic redox potentials of hemes 1 and 3. The NMR signals of the axial ligands of hemes 1 and 3 were also affected. Analysis of the nature of the mutations revealed that a hydrophobic environment and aromaticity are important for the reduction of the redox potentials of hemes 1 and 3, respectively. There was also a global effect. The replacement of Tyr66 with leucine induced chemical shift changes for heme 4, and changes in the microscopic redox potentials of heme 4. The mutations of Tyr65 induced changes in the chemical shifts and microscopic redox potentials for every heme, suggesting that Tyr65 stabilizes the global conformation, thereby reducing the redox potentials. In contrast, although the mutations of His67 and Phe76 caused chemical shift changes for heme 2, they did not affect its redox potentials, showing these residues are not important. All noncoordinated aromatic residues conserved in the cytochrome c_3 subfamily with heme binding motifs CXXCH, CXXXXCH, CXXCH, and CXXXXCH (Phe20, Tyr43, and Tyr66) are involved in the $\pi-\pi$ interaction, which causes a decrease in the redox potential of the interacting heme. The global effect can be attributed to either direct or indirect interactions among the four hemes in the cyclic architecture.

Cytochrome c_3 isolated from sulfate-reducing bacteria is a small soluble protein (typically ca. 14 kDa) and possesses four *c*-type hemes per molecule. This protein has been classified as a class III *c*-type cytochrome (*1*). It is an electron transport protein and plays an important role in sulfate respiration. The three-dimensional structures of various cytochromes c_3 (cyt c_3) (*2* and references therein) and *c*-type multiheme cytochromes in the same superfamily have been determined. The latter include triheme cyt c_7 (*3*), octaheme cyt c_3 (*4*, *5*), nonaheme cyt *c* (*6*, *7*), and hexadecaheme cyt *c* (*8*−*10*). The cyt c_3 family can be divided into four groups based on their heme binding motifs, as shown in Figure 1. The level of homology is highest for the group that has heme binding motifs CXXCH, CXXXXCH, CXXCH, and CXXXXCH (X is any amino acid) along the sequence (termed the 2−4−2−4 group hereafter). Although the level of sequence identity for the family is as low as 29%, that for the 2−4−2−4 group is 65%. The level of homology is even higher in terms of the three-dimensional structure. When the Cα positions of a cyt c_3 tertiary structure are compared with those for *Desulfovibrio vulgaris* Miyazaki F (*Dv*MF),[1] the level of homology is 100, 92, 92, and 90% for *D. vulgaris* Hildenborough (*Dv*H), *Desulfovibrio desulfuricans* ATCC 27774 (*Dd*A), *D. desulfuricans* Essex 6 (*Dd*E), and *Desulfovibrio gigas* (*Dg*), respectively (*11*). In contrast, they are 69, 70, 69, and 65% for *Desulfomicrobium norvegicum* (*Dmn*), the *Dmn* dimer, the *Dg* dimer, and *Dv*H type II cyt c_3, respectively. Clearly, the 2−4−2−4 group comprises a cyt c_3 subfamily. *Dv*MF cyt c_3 used in this work belongs to this subfamily.

One of the characteristic properties of cyt c_3 is its extremely low oxido-reduction (redox) potential, ranging from −50 to −400 mV. Bis-histidine coordination has been

† This research was partly supported by grants from the Ministry of Education, Science, Technology, Sport and Culture of Japan (CREST) and from the New Energy and Industrial Technology Development Organization.

* To whom correspondence should be addressed: Institute for Protein Research, Osaka University, Yamadaoka, Suita 565-0871, Japan. E-mail: akutsu@protein.osaka-u.ac.jp. Phone: +81-6-6879-8597. Fax: +81-6-6879-8599.

‡ Osaka University.

§ Japan Biological Informatics Consortium.

|| Yokohama National University.

⊥ Current address: Research School of Chemistry, Australian National University, Canberra, ACT 0200, Australia.

[1] Abbreviations: NMR, nuclear magnetic resonance; *Dv*MF, *D. vulgaris* Miyazaki F; *Dv*H, *D. vulgaris* Hildenborough; *Dg*, *D. gigas*; *Dd*A, *D. desulfuricans* ATCC 27774; *Dd*E, *D. desulfuricans* Essex 6; *Ds*, *Desulfovibrio salexigens*; *Dd*, *D. desulfuricans*; *Da*, *Desulfovibrio africanus*; *Dmn*, *De. norvegicum*.

10.1021/bi049551i CCC: $27.50
Published on Web 08/06/2004

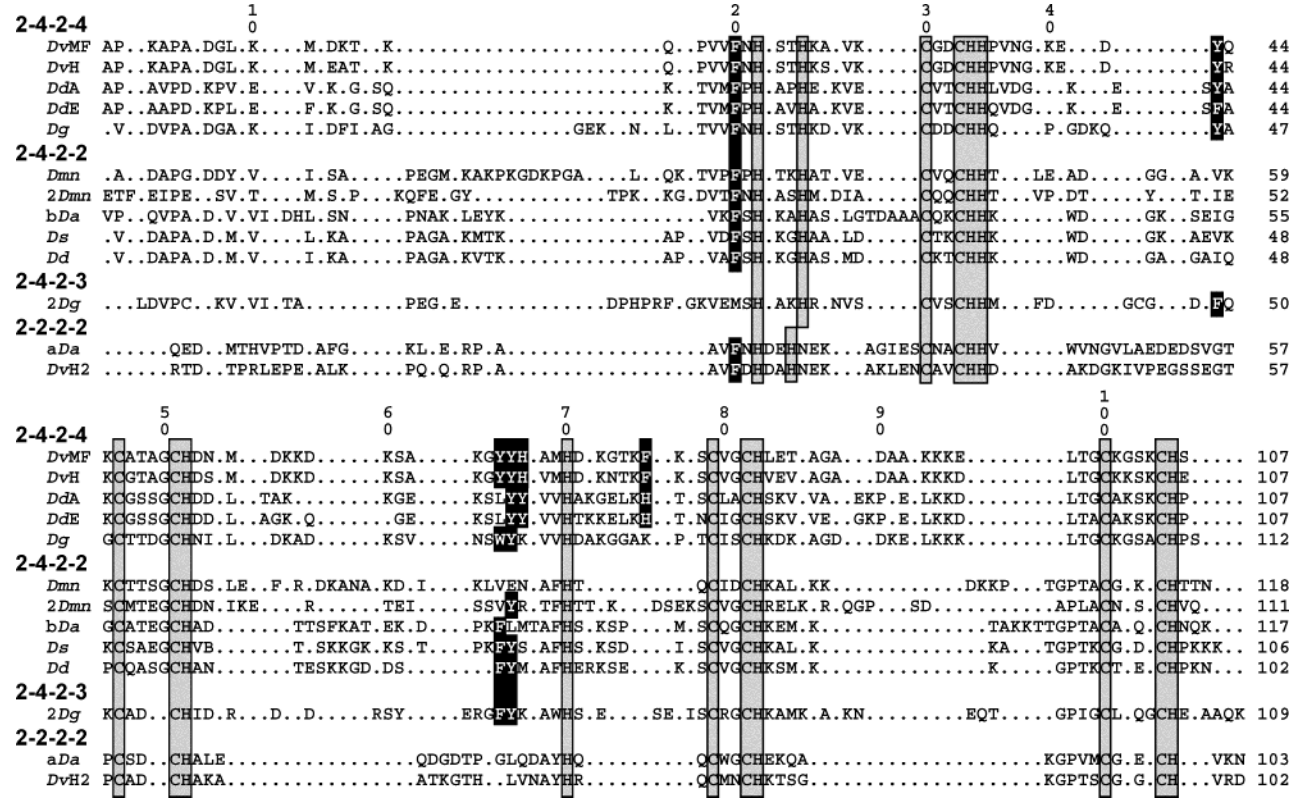

FIGURE 1: Comparison of the amino acid sequences of the cytochrome c_3 family. Members are classified into four groups on the basis of their heme binding motifs, namely, the 2−4−2−4, 2−4−2−2, 2−4−2−3, and 2−2−2−2 groups. The 2−4−2−2 group, for example, stands for cyt c_3 with motifs CXXCH, CXXXXCH, CXXCH, and CXXCH (X is any amino acid) along the sequence. The identical amino acid residues involved in heme binding and coordination are boxed. The amino acid residues considered in this work are highlighted with a black background. The sequence numbers for *Dv*MF are given at the top. Abbreviations: *Dv*H2, *Dv*H type II cyt c_3; 2*Dg*, *Dg* dimer cyt c_3; 2*Dmn*, *Dmn* dimer cyt c_3; a*Da* and b*Da*, acidic and basic cyt c_3 from *D. africanus*, respectively.

identified as one of the major factors in reduction of redox potentials. The contributions of Thr24 (*12*) and Tyr43 (*13*) to the reduction of the redox potentials were indicated by the results of site-directed mutagenesis. The increase in the redox potential caused by mutation was more than 100 mV for heme 3 of T24V cyt c_3 from *Dv*H and more than 40 mV for heme 1 of Y43L cyt c_3 from *Dv*MF. However, there is no clear explanation for the extremely low redox potentials of cyt c_3. Aromatic rings have been suggested to be involved in electron transfer and redox regulation (*13*). Since there are many aromatic residues in cyt c_3, systematic analysis of these residues is important in determining the role of aromatic residues in the reduction of redox potentials. The aromatic residues in *Dv*MF cyt c_3 can be classified into three groups. The aromatic rings of Phe20, Tyr43, Tyr66, and Phe76 are parallel to the imidazole rings of His25 (the sixth ligand of heme 3), His34 (the fifth ligand of heme 1), His70 (the sixth ligand of heme 4), and His35 (the sixth ligand of heme 2), respectively. On the other hand, the side chains of Tyr65 and His67 form hydrogen bonds with the propionate carboxyl groups at C-13 of heme 4 and C-17 of heme 2, respectively. The third group comprises heme ligands (His22, His25, His34, His35, His52, His70, His83, and His106), which are not the subject of this work. In this work, we have examined the roles of the aromatic rings of cyt c_3 in redox regulation in a comprehensive manner, using site-directed mutagenesis, differential pulse polarography, and NMR. The results are discussed in terms of their physicochemical properties and tertiary structures.

MATERIALS AND METHODS

Site-Directed Mutagenesis. All mutations were introduced into the pKFC3k plasmid, which contains the *Dv*MF cyt c_3 gene (*13*). Site-directed mutagenesis was conducted with a Mutan-Super Express Km kit (Takara Shuzo Co., Ltd.) and synthetic oligonucleotides purchased from QIAGEN. The synthetic oligonucleotides used in this study are summarized in Table 1. For the Y43L/Y66L double mutation, the pY43L plasmid (*13*) was digested with *Pst*I and *Eco*RI, and the mutated cyt c_3 gene was ligated to the pKF19k vector (GenBank accession number D63847) at the same restriction sites. Using this vector and the Y66L primer, a second site-directed mutagenesis was carried out as described above. The mutations were confirmed by nucleotide sequencing. This was performed with an ABI PRISM 310 genetic analyzer (Perkin-Elmer), using a DNA sequencing kit, BigDye Terminator Cycle Sequencing Ready Reaction (Applied Biosystems), and two M13 primers, RV-N and M4 (Takara Shuzo Co., Ltd.).

Growth and Purification. Mutated cyt c_3 genes were expressed in *Shewanella oneidensis* TSP-C, as described previously (*14*). ^{15}N-labeled cyt c_3 was produced using ^{15}N-labeled CHL medium (Chlorella Industry Co., Ltd.) supplemented with 46.9 mM fumarate, 31.2 mM lactate, 12.5 mM NaCl, 0.5 mM $MgSO_4$, 0.1 mM $CaCl_2$, 10 μM $FeSO_4$, 5 μM $MnCl_2$, 20 mg/L thiamine hydrochloride, 20 mg/L α-biotin, 20 mg/L adenosine, 20 mg/L guanosine, 20 mg/L cytidine, 20 mg/L thymidine, and 20 mg/L uracil. The transformant was microaerobically grown at 30 °C and then

Table 1: Synthetic Oligonucleotides Used for Site-Directed Mutagenesis[a]

mutation	synthetic oligonucleotide
F20A	5′(244)-CAGCCCGTGGTCGCCAACCACTCGACC-3′(270)
F20E	5′(244)-CAGCCCGTGGTCGAAAACCACTCGACC-3′(270)
F20M	5′(244)-CAGCCCGTGGTCATGAACCACTCGACC-3′(270)
F20H	5′(244)-CAGCCCGTGGTCCACAACCACTCGACC-3′(270)
F20Y	5′(244)-CAGCCCGTGGTCTACAACCACTCGACC-3′(270)
Y65A	5′(378)-GTCCGCCAAGGGCGCCTACCACGCCATGC-3′(406)
Y65F	5′(378)-GTCCGCCAAGGGCTTCTACCACGCCATGC-3′(406)
Y65L	5′(379)-TCCGCCAAGGGCCTCTACCACGCCATG-3′(405)
Y66F	5′(381)-CGCCAAGGGCTACTTCCACGCCATGCATG-3′(409)
Y66L	5′(381)-CGCCAAGGGCTACCTCCACGCCATGCATG-3′(409)
H67A	5′(388)-GGCTACTACGCCGCCATGCATG-3′(409)
H67F	5′(388)-GGCTACTACTTCGCCATGCATG-3′(409)
H67Q	5′(388)-GGCTACTACCAAGCCATGCATG-3′(409)
F76L	5′(415)-GGCACCAAGTTGAAGAGCTGC-3′(435)
F76Y	5′(415)-GGCACCAAGTACAAGAGCTGC-3′(435)

[a] The numbers in parentheses are the sequence numbers according to ref *13*.

harvested. The mutated cyt c_3 was purified as described previously (*15*). The yield was similar to that of wild-type cyt c_3. *Dv*MF was cultured as reported, and [Ni-Fe] hydrogenase was purified from the cells according to the reported method (*16*).

Electrochemical Measurements. Differential pulse polarograms were obtained at 30 °C with a Perkin-Elmer 394 digital electrochemical trace analysis system (Perkin-Elmer), using a dropping mercury electrode and an Ag/AgCl reference electrode. The modulation amplitude, sweep rate, and drop time were 20 mV, 4 mV s^{-1}, and 2 s, respectively. Macroscopic redox potentials were obtained by fitting the analytical equation for four consecutive one-electron reversible electrode reactions to the obtained polarograms (*17*). The macroscopic redox potentials were referred to the standard hydrogen electrode.

NMR Measurements. Samples [0.5−2 mM cyt c_3 in 30 mM sodium phosphate buffer (p^2H 7.0)] were prepared as described previously (*18*). Reduction of cyt c_3 was carried out using a trace of [Ni-Fe] hydrogenase and hydrogen gas. NMR spectra at 500 and 600 MHz were recorded at 303 K with AVANCE DRX-500 and DRX-600 NMR spectrometers (Bruker), respectively. The size of the data set was 2048 × 512. For the assignment of each heme, TOCSY spectra were obtained with a mixing time of 60 ms, and NOESY spectra were acquired with mixing times of 50, 150, and 400 ms in the fully reduced state, as reported previously (*19*). Chemical exchange spectra with a mixing time of 15 ms were recorded for different intermediate oxidation stages to determine the chemical shifts of the heme methyl groups in the fully oxidized (S_0), one-electron-reduced (S_1), two-electron-reduced (S_2), three-electron-reduced (S_3), and fully reduced (S_4) states. The reduction fractions of each heme were determined from the heme methyl chemical shifts in the five macroscopic oxidation states (*20, 21*). For chemical shift perturbation experiments, $^1H-^{15}N$ HSQC spectra were obtained. Chemical shifts are presented in parts per million relative to 2,2-dimethyl-2-silapentane-5-sulfonate (DSS) as an internal reference.

RESULTS

Every aromatic residue of *Dv*MF cyt c_3, except for axial ligands, was mutated. In principle, each was replaced with a different aromatic residue (tyrosine for phenylalanine and vice versa) and with an aliphatic residue, leucine. Other mutations were conducted when needed. The single-amino acid replacements performed in this work are listed in Table 1. In addition, a double mutation, Y43L/Y66L, was introduced. Since mutations F20I (*22*) and F20L (*23*) for *Dv*H cyt c_3 had already been reported, F20A, F20E, F20H, F20M, and F20Y mutations were introduced in an effort to examine the roles of the aromaticity and hydrophobicity of Phe20. Y65A cyt c_3 was produced, since the NMR signals in the two-dimensional chemical exchange spectra of Y65L cyt c_3 were too broad to be analyzed. His67 was replaced with Ala because it is located on the surface. The H67Q mutation was introduced in an effort to examine the role of the hydrogen bond of His67 with the C-17 propionate group of heme 2. Compared with that of wild-type cyt c_3, there were no significant changes in the UV−visible spectra of the fully oxidized and reduced forms of any of the mutants. However, there were changes in ^1H NMR spectra. The chemical shift differences between the wild type and mutants are summarized in Figure 2 for the heme methyl signals at C-18 of heme 1, C-18 of heme 2, C-12 of heme 3, and C-18 of heme 4. Figure 2 indicates that the effects of the mutations are localized to the nearest hemes except in the case of Y65A. The effect was strongest for Phe20.

The four macroscopic redox potentials were determined by differential pulse polarography (DPP) and are summarized in Table 2. In accordance with the chemical shift changes, the effect of the mutation was strongest for Phe20. Among the mutations at Phe20, F20M induced relatively small changes. They were even smaller than those induced by F20Y. Although the Y65L mutation induced a certain increase (32−48 mV) for every step, the Y66L mutation only increased $E_I^{\circ\prime}$ by 25 mV. The Y43L/Y66L double mutation exhibited a stronger effect than the sum of the single mutations. The effects of the mutations at His67 and Phe76 were relatively weak.

The reduction fractions of each heme were calculated using chemical shifts determined from the chemical exchange spectra (*20*). A weak second peak was observed for F20H cyt c_3. The intensity of the minor peak increased at pH 5.0, while the signal disappeared at pH 9.0 (data not shown). This suggests that the appearance of minor peaks can be ascribed to a second protonation of the replaced imidazole. Thus, the imidazole of the major species should carry no

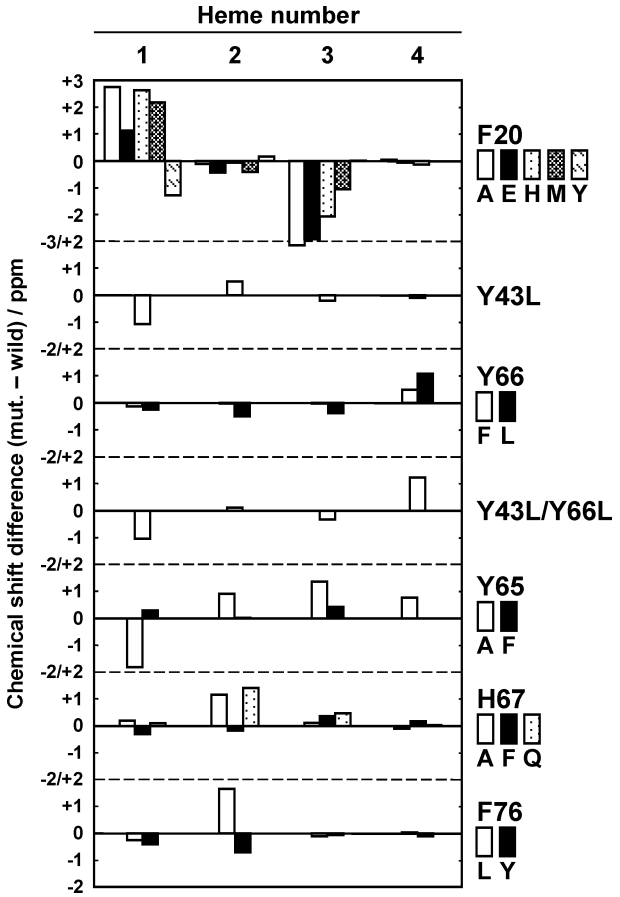

FIGURE 2: Chemical shift changes in the heme methyl signals of the mutated ferricytochrome c_3 in comparison with those of the wild type at p^2H 7.0 and 303 K. The heme methyl signal at C-18 was used for hemes 1, 2, and 4 and that at C-12 for heme 3. The mutation sites and the incorporated amino acid residues are indicated at the right. The lists of the chemical shifts are given in the Supporting Information.

charge. A second peak for each methyl signal also appeared in the alkaline pH region for F20E cyt c_3. This second peak became stronger at higher pH, suggesting that the appearance of second peaks can be ascribed to dissociation of the carboxyl group of Glu20. This led to the conclusion that the carboxyl group of Glu20 is protonated at pH 7.0. Consequently, the replaced His and Glu must carry no charges in the major species at pH 7.0. The hydrophobic environment of the side chain at this position might stabilize the nonionized form rather than the ionized form. The reduction fractions were calculated for the major species.

Microscopic redox potentials were determined using the macroscopic redox potentials and reduction fractions (*21*). The average reduction fractions were calculated under the conditions where $\sum_i R_i^j = \sum_j R_i^j = 1$ (i and j are the heme and reduction step numbers, respectively), using the chemical shifts of signals 2- and 18-CH_3 for heme 1, 7- and 18-CH_3 for heme 2, 12- and 18-CH_3 for heme 3, and 2- and 18-CH_3 for heme 4 (see the Supporting Information). Although Turner et al. (*24*) recommended the use of only one signal for each heme, the chemical shifts of the four signals failed to give the redox potentials because of divergence in the least-squares fitting for the Phe20 and His67 mutants. The microscopic redox potentials at the first reduction step between S_0 and S_1 (e^I) and the fourth reduction step between S_3 and S_4 (e^{IV}) are summarized in Table 3. Typical changes

Table 2: Macroscopic Redox Potentials of the Wild-Type and Mutated Cytochromes c_3 in 30 mM Sodium Phosphate Buffer (pH 7.0) at 30 °C (standard errors of ±2 mV)[a]

	$E_I°'$	$E_{II}°'$	$E_{III}°'$	$E_{IV}°'$
wild type	−242	−296	−313	−358
F20A	−224 (+18)	−255 (+41)	−280 (+33)	−314 (+44)
F20E	−203 (+39)	−238 (+58)	−266 (+47)	−312 (+46)
F20H	−198 (+44)	−239 (+57)	−270 (+43)	−315 (+43)
F20M	−238 (+4)	−269 (+27)	−295 (+18)	−343 (+15)
F20Y	−221 (+21)	−256 (+40)	−281 (+32)	−334 (+24)
Y65A	−227 (+15)	−267 (+29)	−296 (+17)	−335 (+23)
Y65F	−240 (+2)	−290 (+6)	−310 (+3)	−344 (+14)
Y65L	−210 (+32)	−248 (+48)	−278 (+35)	−324 (+34)
Y66F	−247 (−5)	−295 (+1)	−315 (−2)	−356 (+2)
Y66L	−217 (+25)	−288 (+8)	−313 (0)	−358 (0)
Y43L[b]	−232 (+10)	−271 (+25)	−303 (+10)	−350 (+8)
Y43L/Y66L	−198 (+44)	−255 (+41)	−290 (+23)	−344 (+14)
H67A	−251 (−9)	−299 (−3)	−321 (−8)	−361 (−3)
H67F	−246 (−4)	−292 (+4)	−319 (−6)	−361 (−3)
H67Q	−243 (−1)	−292 (+4)	−315 (−2)	−356 (+2)
F76L	−238 (+4)	−283 (+13)	−316 (−3)	−360 (−2)
F76Y	−234 (+8)	−284 (+12)	−313 (0)	−354 (+4)

[a] $E_i°'$ (i = I−IV) is the macroscopic redox potential at the ith reduction step relative to the standard hydrogen electrode (SHE). [b] From ref *13*.

caused by mutation are illustrated in Figure 3. The microscopic redox potentials can provide clear information about the effect of a mutation on each heme in contrast to the macroscopic redox potentials. The microscopic redox potentials of *Dv*MF cyt c_3 exhibit a pH dependence in the neutral pH region. It has been shown that the propionate group of heme 1 at C-13 is mainly responsible for the pH dependence in this region (*21*). The pK_a value of the propionate would not be affected directly by the replacement of aromatic residues. This was actually confirmed by the mutation at Tyr43 (*13*). Therefore, we can analyze the changes in redox potentials as the effects of mutations.

The effect is strongest for the mutation at Phe20. This is consistent with the greatest changes in the heme methyl chemical shifts (Figure 2), and the highest level of conservation of this residue in the primary sequence of cyt c_3 (Figure 1). Although the aromatic ring of Phe20 is parallel to the porphyrin ring of heme 1 and the imidazole ring of the sixth ligand of heme 3 (His25), the effect of the mutation is more significant for heme 1 (Figure 3). Furthermore, the effect on heme 1 is strongest (60−90 mV) for the replacements with polar amino acids (F20E, F20H, and F20Y). Thus, it can be concluded that hydrophobicity is more important than aromaticity for heme 1 at this site. In contrast, the redox potentials of heme 3 are hardly affected by the F20Y mutation, suggesting that aromaticity is important for heme 3. The effects of F20A, F20E, and F20H mutations on heme 3 (35−50 mV) are similar to the effect of the Y43L mutation on heme 1 (*13*). Interestingly, for heme 3, His behaves like a nonaromatic residue while Met behaves like an aromatic residue. Although the effect of F20A on heme 3 is weak in the fully oxidized state, the reason would be different from that in the case of F20M and F20Y. It should be pointed out that nontrivial changes were also induced for hemes 2 and 4. This can be ascribed to a global change in the structural packing induced by a packing deficiency at position 20.

Microscopic redox potentials could not be obtained for Y65L cyt c_3 because of signal broadening in the intermediate oxidation states, S_2−S_4. Even the Y65A mutation caused two

Table 3: Microscopic Redox Potentials at the First and Fourth Reduction Steps (e_i^{I} and e_j^{IV}, respectively)[a] Measured at pH 7.0 and 30 °C

	e_1^{I}	e_2^{I}	e_3^{I}	e_4^{I}	e_1^{IV}	e_2^{IV}	e_3^{IV}	e_4^{IV}
wild type[b]	−309	−325	−285	−252	−292	−315	−344	−307
F20A	−273 (+36)	−295 (+30)	−283 (+3)	−234 (+17)	−244 (+47)	−278 (+36)	−298 (+47)	−264 (+44)
F20E	−226 (+82)	−288 (+37)	−250 (+35)	−228 (+24)	−218 (+74)	−274 (+40)	−297 (+47)	−266 (+42)
F20H	−213 (+95)	−299 (+26)	−236 (+49)	−242 (+10)	−216 (+75)	−285 (+30)	−292 (+52)	−278 (+29)
F20M	−278 (+31)	−312 (+13)	−306 (−21)	−249 (+3)	−249 (+37)	−281 (+34)	−338 (+6)	−277 (+30)
F20Y	−246 (+63)	−306 (+20)	−290 (−5)	−239 (+13)	−229 (+62)	−277 (+37)	−327 (+17)	−271 (+36)
Y65A	−268 (+40)	−208 (+17)	−253 (+32)	−252 (−1)	−264 (+28)	−302 (+12)	−315 (+29)	−291 (+17)
Y65F	−307 (+2)	−327 (−2)	−272 (+13)	−254 (−2)	−282 (+9)	−304 (+10)	−326 (+18)	−300 (+7)
Y66F	−315 (−7)	−332 (−6)	−298 (−13)	−255 (−3)	−286 (+5)	−315 (0)	−343 (+1)	−300 (+7)
Y66L	−341 (−33)	−312 (+13)	−294 (−9)	−219 (+32)	−296 (−4)	−312 (+3)	−349 (−5)	−264 (+44)
Y43L[c]	−265 (+44)	−301 (+24)	−273 (+13)	−254 (−2)	−274 (+17)	−309 (+6)	−336 (+8)	−301 (+6)
Y43L/Y66L	−262 (+47)	−281 (+44)	−269 (+16)	−204 (+48)	−278 (+13)	−300 (+14)	−335 (+9)	−253 (+54)
H67A	−316 (−8)	−341 (−16)	−292 (−7)	−261 (−9)	−291 (+1)	−331 (−17)	−342 (+2)	−308 (−1)
H67F	−306 (+3)	−327 (−2)	−293 (−8)	−256 (−4)	−286 (+5)	−327 (−13)	−346 (−2)	−303 (+5)
H67Q	−306 (+3)	−329 (−4)	−285 (+1)	−254 (−2)	−286 (+6)	−323 (−8)	−339 (+6)	−304 (+3)
F76L	−306 (+3)	−326 (−1)	−281 (+4)	−247 (+4)	−299 (−8)	−328 (−13)	−342 (+2)	−303 (+5)
F76Y	−298 (+10)	−315 (+10)	−279 (+6)	−244 (+8)	−289 (+2)	−314 (0)	−339 (+5)	−301 (+6)

[a] Subscripts denote heme numbers. [b] Recalculated from the data reported in ref *20*. [c] Recalculated from the data reported in ref *13*.

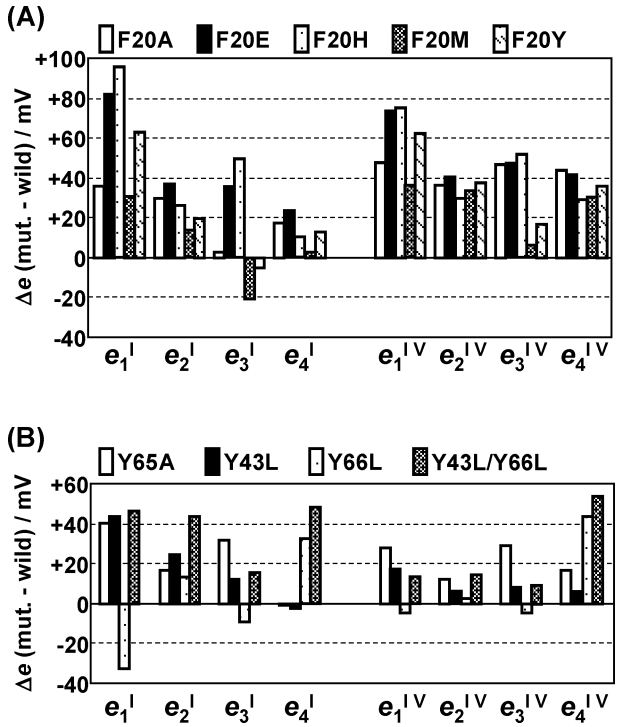

FIGURE 3: Differences in the microscopic redox potentials (e_i^j where i is the heme number and j the reduction step) between the wild-type and mutant cytochrome c_3: (A) mutation at Phe20 and (B) mutation at Tyr43, Tyr65, and Tyr66. The types of mutations are indicated at the top.

peaks in the fully reduced state. The average chemical shifts were used for the fully reduced state to obtain the reduction fractions. The effect of mutation Y65A was not local. Tyr65 is located inside the protein. Therefore, replacement of an aromatic amino acid with a nonaromatic residue would cause a slight but overall structural change because of perturbation of the structural packing, resulting in changes in the redox potentials of all hemes rather than a local one. In the case of the Y66L mutation, the loss of the $\pi-\pi$ interaction between Tyr66 and His70 (the sixth ligand of heme 4) caused an increase in the redox potentials of heme 4 (30−40 mV), like in the case of the Y43L mutation (*13*). As expected from the macroscopic redox potentials, there were no significant changes in the microscopic redox potentials for the mutations at His67 and Phe76. Since the effect of Y65A on heme 4 and that of H67F on heme 2 are weak, the hydrogen bonds involving these aromatic rings are either insignificant for redox regulation or broken in solution. The effect of a double mutation, Y43L/Y66L, was stronger than the sum of the local effects of the single mutations, as in the case of the macroscopic redox potentials. These observations suggest that although the major effects of the mutations at Tyr43 and Tyr66 are local, global effects cannot be neglected. The global effects seem not to be additive.

Wild-type, F20A, and F20H cyt c_3 were uniformly labeled with ^{15}N. Chemical shift perturbations in the $^1H-^{15}N$ HSQC spectrum of ^{15}N-labeled cyt c_3 induced by the F20A or F20H mutation were examined in the fully oxidized and reduced states. The assignment of the signals of the wild type has been reported elsewhere (BMRB accession number 5333 for the reduced form and unpublished data for the oxidized form). The chemical shift changes are more or less the same for these two mutants and two oxidation states. The perturbed regions for the fully oxidized form of F20A cyt c_3 are mapped on the tertiary structure in Figure 4A. The perturbations are mainly located around hemes 1 and 3. This is in good agreement with the chemical shift changes of the heme methyl signals in Figure 2. It is also consistent with the crystal structure of *Dv*H F20L cyt c_3 (*23*), where the structure from L9 to F20, including a β-sheet, is changed in comparison with that of the wild type. This gives us an idea about the conformational changes induced by mutations F20A and F20H. A $^1H-^{15}N$ HSQC spectrum of the axial imidazoles in the fully reduced state is presented in Figure 5. The signals of the fifth (His34) and sixth (His22) ligands of heme 1 are shifted, and those of heme 3 (His83 and His25) have disappeared in the spectrum of the F20A mutant. The former are more shifted, but the signal of the fifth (His83) ligand of heme 3 has been recovered for the F20H mutant. These chemical shift changes of heme 1 ligands are consistent with the order of the redox potential changes of heme 1 for F20A and F20H (Figure 3).

In summary, the mutations at Phe20 induced large chemical shift changes for hemes 1 and 3, and large changes in $E_{II}^{\circ\prime}$ and $E_{IV}^{\circ\prime}$, and e_1^{I}, e_3^{I}, e_1^{IV}, and e_3^{IV}, showing that hemes 1 and 3 are mainly affected by the mutations. It is known that hemes 1−4 are mainly responsible for $E_{II}^{\circ\prime}$, $E_{III}^{\circ\prime}$, $E_{IV}^{\circ\prime}$,

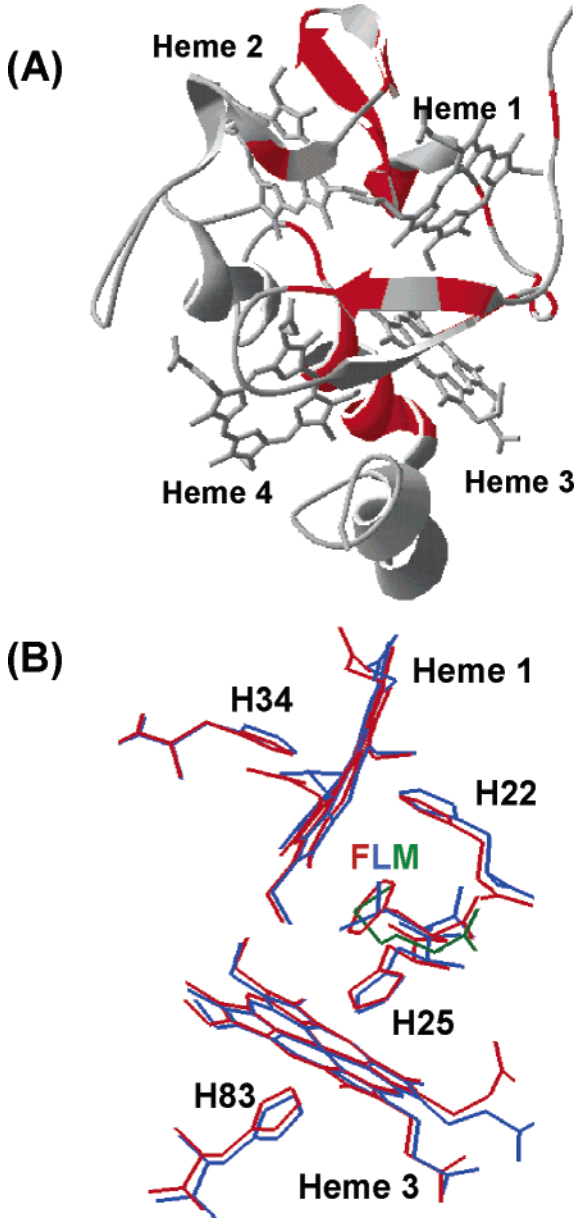

FIGURE 4: (A) Residues showing large perturbations ($\{[(\delta H)^2 + (\delta N/5)^2]/2\}^{1/2} > 0.1$) in the $^1H-^{15}N$ HSQC spectrum of the oxidized F20A cytochrome c_3 are mapped on the tertiary structure (*13*) in red. The figure was prepared with Swiss-PdbViewer (*28*). (B) Crystal structures around hemes 1 and 3. The two structures are superimposed in such a way that the four hemes are best fitted. Red and blue lines denote *Dv*H wild-type (PDB entry 2CTH) and F20L (PDB entry 1MDV) cyt c_3, respectively. The side chain of Met in *Dg* dimer cyt c_3 (PDB entry 1GYO) is shown in green. This figure was prepared with MOLMOL (*29*).

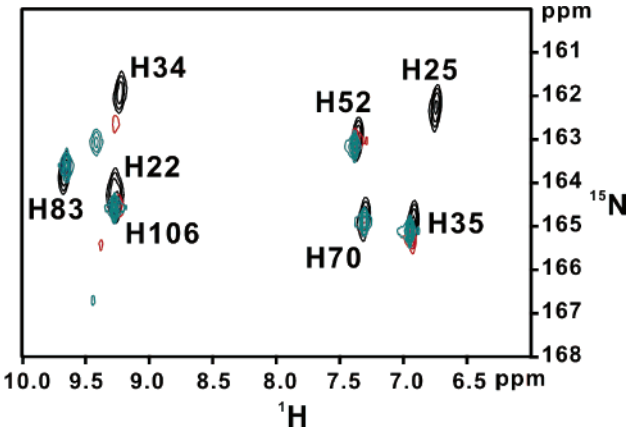

FIGURE 5: Imide signals of the axial imidazoles in the $^1H-^{15}N$ HSQC spectrum of the fully reduced form at 600 MHz, pH 7.0, and 303 K. Black, red, and blue show data for the wild-type, F20A, and F20H cytochrome c_3, respectively. H34, H52, H83, and H106 are the fifth ligands and H22, H35, H25, and H70 the sixth ligands of hemes 1−4, respectively.

and $E_1°'$, respectively (*21*). Additional changes were also seen for e_2 and e_4. The chemical shift perturbation experiments showed that the axial ligands of hemes 1 and 3 are affected by mutations. Analysis of the nature of the mutations revealed that a hydrophobic environment and aromaticity are important for redox regulation of hemes 1 and 3, respectively. Nevertheless, the effect of a mutation comprises a combination of local and global ones. The replacement of Tyr66 with leucine induced chemical shift changes for heme 4, and changes in $E_1°'$, e_4^I, and e_4^{IV} of 25, 32, and 44 mV, respectively, suggesting that aromatic rings contribute to the reduction of the redox potentials of heme 4. The mutations at Tyr65 induced changes in the chemical shifts and microscopic redox potentials for every heme and ones in the macroscopic redox potentials for every step, suggesting that Tyr65 stabilizes the global conformation, thereby lowering the redox potentials. In contrast, although the mutations at His67 and Phe76 caused chemical shift changes for heme 2, they did not affect the redox potentials, showing these residues are not important for redox regulation.

DISCUSSION

The effect of amino acid replacement on the redox potentials was strong for Phe20, Tyr43, Tyr65, and Tyr66, but weak for His67 and Phe76. As can be seen in Figure 1, Phe20, Tyr43, and Tyr66 are conserved in the 2−4−2−4 subfamily of cyt c_3. Of the aromatic residues parallel to the axial ligands, only conserved ones exhibited large contributions to the reduction of the redox potentials. The conservation of a hydrophobic residue at position 65 indicates that this residue should contribute to the structural packing inside of the protein. Although His76 (corresponding to Phe76 in *Dv*MF cyt c_3) has been indicated as being important in *Dd*A cyt c_3 (*25*), it is not conserved in the 2−4−2−4 subfamily and its contribution to the redox potentials are minor in *Dv*MF cyt c_3. Why is the contribution of Phe76 different from those of Phe20, Tyr43, and Tyr66? The angle of the two ligated imidazole planes of heme 2 is 64°, while it is less than 10° for the other hemes (*13*, *26*). The $Fe-N_{\epsilon 2}$ lengths of heme 2 are also long, suggesting that the coordination strengths are weaker than the others. The weak coordination might be the reason Phe76 is not effective in reducing the redox potentials.

The reduction fractions of the F20A and F20M mutants are similar to those of *Dv*H F20I cyt c_3 (*22*). Their macroscopic redox potentials are also consistent with those of *Dv*H F20L cyt c_3 (*23*). It turned out that a hydrophobic environment is important for heme 1 to keep the redox potential low. The $^1H-^{15}N$ HSQC spectra of the imidazole groups indicate that a mutation at this position causes chemical shift changes in the ligand signals of heme 1 (Figure 5). The change is greater for F20H than for F20A. In the crystal structure of *Dv*H F20L cyt c_3, replacement of the side chain induces a slight change in the orientation of the

porphyrin ring of heme 1 (Figure 4B), presumably due to the elimination of its stacking with the phenyl group of Phe20 (*23*). These facts strongly suggest that a hydrophilic side chain at this position facilitates the change in the porphyrin orientation of heme 1, resulting in a change in the coordination structure of its axial ligands. The weaker intensity (because of line broadening) and larger shift of the His22 signal, compared to those of the His34 one in Figure 5, suggest that the change in the coordination is greater for the sixth ligand than the fifth one, in accordance with Figure 4B. In contrast to heme 1, the redox potentials of heme 3 are lowered by $\pi-\pi$ interactions. The effect of F20M on the redox potentials of heme 3 was similar to that of F20Y, suggesting that Met behaves like an aromatic residue. Only *Dg* dimer cyt c_3 carries Met at the Phe20 site. In its crystal structure (*5*), the sulfur of Met is located at the position of the phenyl ring of Phe20 (Figure 4B). The factors mentioned above caused local effects. It has already been indicated that the structure in this region stabilizes the folding of the protein (*23*). This will contribute to the global changes in the redox potentials induced by the replacement of Phe20. The difference in global changes in the fully oxidized and reduced states should have something to do with the conformational change in *Dv*MF cyt c_3 during the redox process (*2*). Consequently, the compact and double stacking structure formed by heme 1, Phe20, and His25 should be one of the important factors for the extremely low redox potentials of cyt c_3.

It can be concluded that the effect of amino acid replacement on the redox potentials of each heme comprises a combination of local and global ones. All conserved aromatic rings contribute to the decrease in the redox potentials of the local heme through the $\pi-\pi$ interaction by 30−50 mV. The double stacking structure in the region of hemes 1 and 3 can contribute to the reduction of the redox potentials by up to 100 mV. The global effect can be attributed to either direct or indirect interactions among the four hemes. Actually, it was indicated that the cyclic architecture of the four hemes is important for the extremely low redox potentials of cyt c_3 in light of the redox properties of the linear architecture in a small tetraheme cytochrome *c* (STC) (*27*). The latter has bi-imidazole coordinated *c*-type hemes such as cyt c_3, and a much lower pI and much greater heme exposure than in the case of cyt c_3, which are supposed to make the redox potentials of STC lower than those of cyt c_3. In reality, however, its redox potentials are higher than those of cyt c_3 by ∼100 mV on average.

ACKNOWLEDGMENT

We are grateful to Prof. Takahisa Ikegami (Osaka University) for the help and fruitful discussions regarding the NMR measurements.

SUPPORTING INFORMATION AVAILABLE

Chemical shift tables of the heme methyl signals of all mutant proteins used in this work in the five oxidation states. This material is available free of charge via the Internet at http://pubs.acs.org.

REFERENCES

1. Ambler, R. P. (1980) in *From Cyclotrons to Cytochromes* (Robinson, A. B., and Kaplan, N. O., Eds.) pp 263−279, Academic Press, London.
2. Harada, E., Fukuoka, Y., Ohmura, T., Fukunishi, A., Kawai, G., Fujiwara, T., and Akutsu, H. (2002) Redox-coupled conformational alterations in cytochrome c_3 from *D. vulgaris* Miyazaki F on the basis of its reduced solution structure, *J. Mol. Biol. 319*, 767−778.
3. Czjzek, M., Arnoux, P., Haser, R., and Shepard, W. (2001) Structure of cytochrome c_7 from *Desulfuromonas acetoxidans* at 1.9 Å resolution, *Acta Crystallogr. D57*, 670−678.
4. Czjzek, M., Guerlesquin, F., Bruschi, M., and Haser, R. (1996) Crystal structure of a dimeric octaheme cytochrome c_3 (M_r 26000) from *Desulfovibrio desulfuricans* Norway, *Structure 4*, 395−404.
5. Frazão, C., Sieker, L., Sheldrick, G., Lamzin, V., LeGall, J., and Carrondo, M. A., (1999) *Ab initio* structure solution of a dimeric cytochrome c_3 from *Desulfovibrio gigas* containing disulfide bridges, *J. Biol. Inorg. Chem. 4*, 162−165.
6. Matias, P. M., Coelho, R., Pereira, I. A. C., Coelho, A. V., Thompson, A. W., Sieker, L. C., LeGall, J., and Carrondo, M. A. (1999) The primary and three-dimensional structures of a nine-haem cytochrome *c* from *Desulfovibrio desulfuricans* ATCC 27774 reveal a new member of the Hmc family, *Structure 7*, 119−130.
7. Umhau, S., Fritz, G., Diederichs, K., Breed, J., Welte, W., and Kroneck, P. M. H. (2001) Three-Dimensional Structure of the Nonaheme Cytochrome *c* from *Desulfovibrio desulfuricans* Essex in the Fe(III) State at 1.89 Å Resolution, *Biochemistry 40*, 1308−1316.
8. Matias, P. M., Coelho, A. V., Valente, F. M. A., Plácido, D., LeGall, J., Xavier, A. V., Pereira, I. A. C., and Carrondo, M. A. (2002) Sulfate respiration in *Desulfovibrio vulgaris* Hildenborough: Structure of the 16-heme Cytochrome *c* HmcA at 2.5 Å resolution and a view of its role in transmembrane electron transfer, *J. Biol. Chem. 277*, 47907−47916.
9. Czjzek, M., ElAntak, L., Zamboni, V., Morelli, X., Dolla, A., Guerlesquin, F., and Bruschi, M. (2002) The Crystal Structure of the Hexadeca-Heme Cytochrome Hmc and a Structural Model of its Complex with Cytochrome c_3, *Structure 10*, 1677−1686.
10. Sato, M., Shibata, N., Morimoto, Y., Takayama, Y., Ozawa, K., Akutsu, H., Higuchi, Y., and Yasuoka, N. (2004) X-ray induced reduction of the crystal of high-molecular weight cytochrome *c* revealed by microspectrometry, *J. Synchrotron Radiat. 11*, 113−116.
11. Aragão, D., Frazão, C., Sieker, L., Sheldrick, G. M., LeGall, J., and Carrondo, M. A. (2003) Structure of dimeric cytochrome c_3 from *Desulfovibrio gigas* at 1.2 Å resolution, *Acta Crystallogr. D59*, 644−653.
12. Salgueiro, C. A., da Costa, P. N., Turner, D. L., Messias, A. C., van Dongen, W. M. A. M., Saraiva, L. M., and Xavier, A. V. (2001) Effect of hydrogen-bond networks in controlling reduction potentials in *Desulfovibrio vulgaris* (Hildenborough) cytochrome c_3 probed by site-specific mutagenesis, *Biochemistry 40*, 9709−9716.
13. Ozawa, K., Takayama, Y., Yasukawa, F., Ohmura, T., Cusanovich, M. A., Tomimoto, Y., Ogata, H., Higuchi, Y., and Akutsu, H. (2003) Role of the aromatic ring of Tyr43 in tetraheme cytochrome c_3 from *Desulfovibrio vulgaris* Miyazaki F, *Biophys. J. 85*, 3367−3374.
14. Ozawa, K., Yasukawa, F., Fujiwara, Y., and Akutsu, H. (2001) A Simple, Rapid, and Highly Efficient Gene Expression System for Multiheme Cytochrome *c*, *Biosci., Biotechnol., Biochem. 65*, 185−189.
15. Ozawa, K., Tsapin, A. I., Nealson, K. H., Cusanovich, M. A., and Akutsu, H. (2000) Expression of a Tetraheme Protein, *Desulfovibrio vulgaris* Miyazaki F Cytochrome c_3, in *Shewanella oneidensis* MR-1, *Appl. Environ. Microbiol. 66*, 4168−4171.
16. Yagi, T., and Maruyama, K. (1971) Purification and properties of cytochrome c_3 of *Desulfovibrio vulgaris*, Miyazaki, *Biochim. Biophys. Acta 243*, 214−224.
17. Niki, K., Kobayashi, Y., and Matsuda, H. (1984) Determination of macroscopic standard potentials of a molecule with a reversible *n*-consecutive one-electron-transfer process. Application to a tetraheme protein: cytochrome c_3, *J. Electroanal. Chem. 178*, 333−341.
18. Park, J.-S., Kano, K., Niki, K., and Akutsu, H. (1991) Full assignment of heme redox potentials of cytochrome c_3 of *D. vulgaris* Miyazaki F by ^{1}H-NMR, *FEBS Lett. 285*, 149−151.
19. Ohmura, T., Inobe, T., Kano, K., Horizumi, T., and Akutsu, H. (1997) Unusual behavior of a heme in a tetraheme protein,

cytochrome c_3 from *Desulfovibrio vulgaris* Miyazaki F, in the reduction process, *J. Electroanal. Chem. 438*, 237−243.
20. Fan, K., Akutsu, H., Kyogoku, Y., and Niki, K. (1990) Estimation of microscopic redox potentials of a tetraheme protein, cytochrome c_3 of *Desulfovibrio vulgaris*, Miyazaki F, and partial assignments of heme groups, *Biochemistry 29*, 2257−2263.
21. Park, J.-S., Ohmura, T., Kano, K., Sagara, T., Niki, K., Kyogoku, Y., and Akutsu, H. (1996) Regulation of the redox order of four hemes by pH in cytochrome c_3 from *D. vulgaris* Miyazaki F, *Biochim. Biophys. Acta 1293*, 45−54.
22. Saraiva, L. M., Salgueiro, C. A., LeGall, J., van Dongen, W. M. A. M., and Xavier, A. V. (1996) Site-directed mutagenesis of a phenylalanine residue strictly conserved in cytochrome c_3, *J. Biol. Inorg. Chem. 1*, 542−550.
23. Dolla, A., Arnoux, P., Protasevich, I., Lobachov, V., Bruhna, M., Giudici-Orticoni, M. T., Haser, R., Czjzek, M., Makarov, A., and Bruschi, M. (1999) Key Role of Phenylalanine 20 in Cytochrome c_3: Structure, Stability, and Function Studies, *Biochemistry 38*, 33−41.
24. Turner, D. L., Salgueiro, C. A., Catarino, T., LeGall, J., and Xavier, A. V. (1996) NMR studies of cooperativity in the tetrahaem cytochrome c_3 from *Desulfovibrio vulgaris*, *Eur. J. Biochem. 241*, 723−731.
25. Bento, I., Matias, P. M., Baptista, A. M., da Costa, P. N., van Dongen, W. M. A. M., Saraiva, L. M., Schneider, T. R., Soares, C. M., and Carrondo, M. A. (2004) Molecular basis for redox-bohr and cooperative effects in cytochrome c_3 From *Desulfovibrio desulfuricans* ATCC 27774: Crystallographic and modeling studies of oxidized and reduced high-resolution structures at pH 7.6, *Proteins 54*, 135−152.
26. Higuchi, Y., Kusunoki, M., Matsuura, Y., Yasuoka, N., and Kakudo, M. (1984) Refined structure of cytochrome c_3 at 1.8 Å resolution, *J. Mol. Biol. 172*, 109−139.
27. Harada, E., Kumagai, J., Ozawa, K., Imabayashi, S., Tsapin, A. S., Nealson, K. H., Meyer, T. E., Cusanovich, M. A., and Akutsu, H. (2002) A directional electron transfer regulator based on heme-chain architecture in the small tetraheme cytochrome *c* from *Shewanella oneidensis*, *FEBS Lett. 532*, 333−337.
28. Guex, N., and Peitsch, M. C. (1996) Swiss-PDBViewer: A fast and easy-to-use PDB viewer for Macintosh and PC, *Protein Data Bank Quarterly Newsletter 77*, 7.
29. Koradi, R., Billeter, M., and Wüthrich, K. (1996) MOLMOL: A program for display and analysis of macromolecular structures, *J. Mol. Graphics 14*, 51−55.

BI049551I